Pharmacology & Toxicology Research

https://acadpub.com/ptr

Nanocomposites of AS1411 and Novel Drug for Targeted Cancer Therapy

[1]Hafiz Muhammad Yameen, [2]Ishba Mahmood, [3]Sittara

[1]Department of Pharmaceutics, GC University, Faisalabad, Pakistan
[2]Skims Pharmaceuticals, khurrianwala, Faisalabad, Pakistan
[3]A&K Pharmaceuticals, Faisalabad, Pakistan

About the Article

Open Access

Research Article

How to Cite: Hafiz Muhammad Yameen, Ishba Mahmood, Sittara. Nanocomposites of AS1411 and Novel Drug for Targeted Cancer Therapy. Pharmacol. Toxicol. Res. 2025;1:11–23.

Keywords:
Cancer, drug, nanocomposites, therapy

Corresponding author:
Hafiz Muhammad Yameen,
Department of Pharmaceutics, GC University, Faisalabad, Pakistan

ABSTRACT

Background and Objective: Breast cancer remains a prevalent health challenge, underscoring the need for advanced therapeutic strategies that maximize efficacy while minimizing side effects. This study aimed to develop and characterize gelatin-based nanoparticles as carriers to improve efficacy and reduce side effects by using targeted delivery (Due to aptamer-AS1411) of anticancer potential of novel drug (SA24-3) in conjunction with photosensitizer (Chlorine e6) as photodynamic therapy (PDT) for synergistic effect. A factorial design was employed to optimize nanoparticle formulation.

Materials and Methods: Comprehensive characterization of the nanoparticles included particle size, zeta potential, and morphological assessments using Scanning Electron Microscopy (SEM), confirming smooth, spherical particles. Fourier-transform Infrared Spectroscopy (FTIR) and X-ray diffraction (XRD) were conducted to validate drug incorporation and assess molecular interactions, confirming the amorphous state of the encapsulated drugs. Cytotoxicity was evaluated against the MCF-7 breast cancer cell line using the MTT assay, confirming significant anticancer activity. The chick chorioallantoic membrane (CAM) assay and RBC aggregation studies under PDT conditions revealed effective anti-angiogenic properties and enhanced oxygen delivery, crucial for photodynamic efficacy. Additionally, *in vivo* toxicity assessment demonstrated no adverse effects on blood parameters or major organs, reinforcing the formulation's safety profile.

Results: The characterization results confirmed smooth, spherical nanoparticles with suitable size and charge for targeted delivery. The FTIR and XRD analyses validated successful drug encapsulation and molecular interaction. Cytotoxicity studies demonstrated significant anticancer activity against the MCF-7 cell line. CAM and RBC aggregation assays indicated potent anti-angiogenic effects and enhanced oxygenation under PDT conditions, while *in vivo* toxicity evaluation showed no harmful effects on blood or organ systems.

Conclusion: This research work demonstrates the potential of aptamer (AS1411) guided Novel anti-cancer drug (SA24-3) and Chlorine E6 loaded polymeric nanoparticles as a multifaceted and targeted approach for breast cancer treatment, leveraging biocompatibility and photodynamic synergy to improve therapeutic outcomes. These findings provide a foundation for further clinical investigations, with the potential to impact future breast cancer therapy.

INTRODUCTION

Cancer is a complex group of diseases characterized by uncontrolled and abnormal cell growth that can spread throughout the body. The term “cancer” encompasses a wide range of illnesses with diverse characteristics and symptoms that may develop in nearly any organ or tissue. Despite this diversity, most cancers share fundamental features such as genetic mutations that disrupt normal cell division and

survival mechanisms. Among these, breast cancer remains one of the most prevalent malignancies in women and continues to contribute significantly to global mortality rates. It is a molecularly heterogeneous disease characterized by uncontrolled proliferation of abnormal breast tissue cells.

Breast cancer is broadly classified into two categories: early-stage and advanced-stage. Early-stage breast cancer refers to tumors confined to the breast tissue or those that have spread only to the nearby axillary lymph nodes and it is often considered curable with timely treatment. In contrast, advanced-stage breast cancer, which may involve distant metastasis, is not completely curable but can be managed through symptom-control strategies and targeted therapies[1].

Over recent years, therapeutic strategies have evolved considerably, shifting from generalized chemotherapy toward biologically directed and targeted therapies. The goal of these approaches is to enhance treatment efficacy while minimizing adverse effects by sparing normal, healthy tissues. For instance, women with metastatic hormone receptor-positive breast cancer are preferentially treated with hormonal therapy and patients exhibiting any level of hormonal receptor positivity are advised to receive such therapy[2].

However, monotherapy using a single therapeutic agent has been found to be largely ineffective in many cases, mainly due to the development of drug resistance and enhanced toxicity. Combination therapies have therefore emerged as a more effective alternative. These may include combinations such as radiation therapy with adjuvant therapy, targeted therapy with immunotherapy and endocrine therapy alongside chemotherapy[3]. In this context, our research proposes a combination approach employing photodynamic therapy (PDT) alongside a novel anticancer drug to achieve a superior antitumor effect.

Photodynamic therapy (PDT) is an advanced, minimally invasive therapeutic technique that relies on a sequence of photochemical and photobiological reactions leading to selective destruction of malignant tissues. The process involves three key components: Light of a specific wavelength, a photosensitizer (PS) and molecular oxygen. Photosensitizers contain chromophores that absorb visible light at specific wavelengths, leading to excitation into unstable higher-energy states. These excited molecules subsequently release energy through fluorescence or internal conversion into heat, resulting in the production of free radicals and Reactive Oxygen Species (ROS). The generated ROS induce necrosis or apoptosis of cancerous cells while leaving normal tissues relatively unharmed.

An ideal photosensitizer must fulfill several criteria: it should be non-toxic to healthy tissues, exhibit high ROS yield and possess absorption within the 600-800 nm spectral window where tissue penetration of light is optimal[4]. In our study, Solvent Green dye will be utilized as the potential photosensitizer owing to its suitable optical properties and photostability.

A major challenge in anticancer therapy, however, remains the untargeted administration of active compounds. Non-specific distribution of drugs can lead to severe side effects, including cytotoxicity to normal cells and interference with physiological functions. Moreover, oral administration often faces additional limitations such as poor solubility, low bioavailability, non-selectivity and first-pass metabolism. To overcome these issues, nanotechnology-based drug delivery systems have been widely explored.

Nanoparticle-based formulations improve drug dispersion, solubility and cellular uptake while offering enhanced drug loading capacity and the possibility of targeted delivery, thus reducing adverse effects on healthy tissues[5]. Various nanoparticle systems for the anticancer drug letrozole have been previously reported, including folic acid-conjugated solid lipid nanoparticles[6], folic acid-decorated nanoliposomes[7], The PEGylated nanoparticles[8] and other solid lipid nanoparticle systems[9].

In the present research, we aim to develop polymeric nanoparticles for co-delivery of Chlorin E6 (a photosensitizer) and AS1411 (a nucleolin-targeted aptamer). Polymeric nanoparticles are particularly effective for enhancing bioavailability and achieving site-specific drug delivery. Their versatility allows precise control over drug encapsulation, release kinetics and surface modification, making them ideal candidates for customized drug delivery systems[10]. These nanoparticles typically range between 1 and 200 nm and can encapsulate active compounds through entrapment within the polymer matrix or adsorption onto the nanoparticle surface.

The preparation method of polymeric nanoparticles depends on the physicochemical characteristics of the drug and the intended route of administration. Common fabrication techniques include ionic gelation, nanoprecipitation, salting out, solvent evaporation and spray drying. Among these, the oil-in-water (O/W) emulsification solvent evaporation method is one of the most established and effective techniques. This process involves dissolving the polymer and drug in an organic solvent (oil phase), emulsifying it into an aqueous phase containing surfactants and then evaporating the solvent to yield polymeric nanoparticles[11].

Polymeric nanoparticle-based systems offer several advantages, including sustained drug release, improved pharmacokinetics, enhanced stability and the potential for surface modification to achieve active targeting. When used in combination with photodynamic therapy, such systems can enhance localized drug accumulation and phototoxicity within tumor tissues, while minimizing systemic toxicity. This combination approach represents a promising avenue for improved management of resistant or advanced breast cancers.

This study was conducted to prepare and optimize polymeric nanoparticles co-loaded with a novel drug, Chlorin E6 and AS1411. The optimized nanoparticles were characterized *in vitro* by assessing particle size, zeta potential, surface morphology (SEM) and structural and thermal properties (FTIR, TGA, XRD and DSC). Cell viability was evaluated using MTT assays under both light and dark conditions to assess photodynamic effects. The CAM egg model was employed to investigate the angiogenesis effect of the formulation. Furthermore, *in-vivo* antitumor studies were performed to evaluate the therapeutic efficacy of the optimized formulation and fluorescence imaging was utilized to visualize the *in-vivo* biodistribution of the nanoparticles.

MATERIALS AND METHODS

Study design: A random study design was employed due to its simplicity and flexibility, allowing evaluation of various experimental conditions without a structured factorial setup. The independent variables included the concentrations of the novel anti-cancer drug (SA24-3), photosensitizer (Chlorin e6), aptamer (AS1411) and gelatin. The study focused on the synthesis, characterization and evaluation of gelatin based nano particles for anticancer applications.

Preparation of stock solutions

Gelatin stock solution: A 10% w/v gelatin solution was prepared by dissolving 2.5 g of gelatin in 25 mL of distilled water at 50°C under continuous stirring at 700 rpm for 15-20 min. The solution was stored at -20°C until further use.

SA24-3 stock solution: Nineteen milligrams of the novel anti-cancer drug SA24-3 were dissolved in 6.33 mL of distilled water and sonicated for 5 minutes to form a uniform solution, which was stored at -20°C.

Chlorin e6 (Ce6) stock solution: A 20 mg quantity of Chlorin e6 was dissolved in 10 mL of acetone and sonicated for 3 min. The stock solution was stored at -20°C until required.

Preparation of gelatin based nanoparticles

Blank gelatin nanoparticles: Blank gelatin nanoparticles were synthesized using a two-step desolvation method. A 10% w/v gelatin solution was prepared at 50°C. Twenty-five milliliters of acetone were added as a desolvating agent to precipitate high molecular weight gelatin, which got sediment by keeping the solution at room temperature for 10 min. The supernatant was discarded and the gelatin precipitate was re-dissolved in 25 mL distilled water at 50°C. The pH was adjusted to 3 using 6N HCl. Subsequently, 75 mL of acetone was added dropwise under continuous stirring at 50°C to form nanoparticles. Crosslinking was achieved using 0.6 mL of 25% glutaraldehyde, followed by stirring for 2 hrs. The resulting nanoparticles were centrifuged at 4400 rpm for 20 min, washed thrice with acetone : water (3:7) and stored at 4°C.

SA24-3 loaded nanoparticles: The procedure was repeated as above, except 0.33 mL of SA24-3 stock solution was added to the gelatin solution prior to desolvation. A total of 74.67 mL acetone was added dropwise under constant stirring, followed by 0.6 mL glutaraldehyde for crosslinking. The nanoparticles were centrifuged, washed and stored under identical conditions.

Chlorin e6 (Ce6) loaded nanoparticles: Similarly, 0.33 mL of Chlorin e6 stock solution was incorporated into the gelatin solution prior to nanoparticle formation. The same desolvation, crosslinking and purification steps were followed.

SA24-3 and Ce6 Co-loaded nanoparticles: Both 0.33 mL of SA24-3 and 0.33 mL of Ce6 stock solutions were simultaneously added to the gelatin solution before desolvation. Acetone (74.34 mL) was added dropwise and the mixture was crosslinked with 0.6 mL of 25% glutaraldehyde. Nanoparticles were collected by centrifugation, washed and stored at 4°C.

SA24-3, Ce6 and AS1411 loaded nanoparticles: For triple-loaded nanoparticles, 0.33 mL each of SA24-3, Ce6 and AS1411 stock solutions were added sequentially to the gelatin solution. Acetone (74.01 mL) was added dropwise under stirring at 50°C, followed by 0.6 mL glutaraldehyde for crosslinking. The nanoparticles were centrifuged, washed and stored at 4°C for further characterization.

Characterization of nanoparticles: Prepared formulations were subjected to various physicochemical and biological evaluations, including particle size, zeta potential, FTIR, SEM, XRD, TGA, DSC, *in-vitro* cytotoxicity, erythrocyte aggregation, CAM assay and *in-vivo* studies.

Particle size analysis: Particle size distribution and polydispersity index (PDI) were measured using a Zetasizer Nano-ZS (Malvern Instruments, UK) by Dynamic Light Scattering (DLS). Samples were diluted with distilled water and analyzed at 25°C. Measurements were taken in triplicate and mean size distribution was recorded based on intensity.

Zeta potential measurement: Zeta potential was determined using a Litesizer DLS 500 instrument. Samples were diluted in distilled water and analyzed in cuvettes at 25°C to assess surface charge and colloidal stability.

Scanning electron microscopy (SEM): Surface morphology was visualized using SEM (Sigma 300 VP). A few drops of nanoparticle suspension were placed on carbon tape and allowed to dry for 5-10 min. This step was repeated 4-5 times before analysis at 10,000× magnification.

Fourier transform infrared spectroscopy (FTIR): FTIR spectroscopy was employed to determine chemical compatibility and potential interactions among components. Spectra for blank, SA24-3, Ce6, dual- and triple-loaded nanoparticles were recorded in the 500-4000 cm^{-1} wavelength range.

X-ray diffraction (XRD): XRD patterns were obtained using a Rigaku Miniflex II diffractometer (Cu Kα radiation, λ = 1.54 Å). Samples were scanned from 20° to 80° (2θ) at a step size of 0.05° and 2 seconds per step to determine crystalline nature and structural modifications.

Differential scanning calorimetry (DSC): Thermal transitions of formulations F1-F5 were analyzed using DSC. Samples (sealed in aluminum pans) were heated from room temperature to 300°C at 10°C/min. Heat flow curves were recorded to assess thermal behavior and drug–polymer interactions.

Thermogravimetric analysis (TGA): TGA was conducted under nitrogen atmosphere using platinum crucibles. Samples were heated from room temperature to 500°C at 10°C/min. Weight loss patterns were analyzed to determine thermal stability, composition and degradation behavior.

Biological evaluation

Erythrocyte aggregation test: Fresh human blood (5 mL) was centrifuged at 1000 rpm for 5 minutes to separate plasma. RBCs were washed with PBS (pH 7.4) and diluted (1:10). To 900 µL of RBC suspension, 100 µL of formulations F1–F5 were added step by step. PBS served as a negative control and Triton X-100 as a positive control. After incubation, RBC smears were examined microscopically (10×) for aggregation or hemolysis.

***In-vitro* cytotoxicity (MTT assay):** Cytotoxicity was evaluated against MDA-MB-231 breast cancer cells. Cells (10,000/well) were cultured in 96-well plates and incubated at 37°C for 48 hrs. Following treatment with formulations (5 µL), wells were washed with PBS and 10 µL MTT reagent was added. After 3 hrs incubation, formazan crystals were solubilized with 100 µL ethanol and absorbance was recorded at 570 nm using a plate reader. Cell viability (%) was calculated to assess phototoxic and dark toxicity effects[12].

Chorioallantoic membrane (CAM) assay: Anti-angiogenic potential was evaluated using fertilized chicken eggs incubated at 37°C. On day 4, embryos were examined and resealed. On day 9, formulations F1 and F5 were applied to the CAM surface followed by red light exposure at various intervals. Images were taken before and after treatment to assess inhibition of angiogenesis and vascular regression.

In-vivo Cytotoxicity and Toxicological Evaluation

Acute toxicity study: Fifteen healthy albino mice (130-135 g) were divided into five treatment groups (F1-F5) and one control group (n = 2 per group). Formulations (0.5 mL/dose) were administered intraperitoneally on days 1, 3 and 7. After 7 days, mice were sacrificed; blood and organs were collected for hematological, biochemical and histopathological analysis.

Hematology and serum biochemistry: Blood was analyzed for RBC count, hemoglobin, AST, ALT, ALP, bilirubin, urea and creatinine levels. No significant differences were observed compared to control, indicating absence of hepatic or renal toxicity.

Histopathology: Liver, kidney, lung and heart tissues were fixed in 10% formalin and examined microscopically. No signs of necrosis, inflammation, or morphological abnormalities were detected, suggesting good biocompatibility[13].

Tumor induction and photodynamic evaluation in rats: Tumor induction was carried out in 24 rats divided into four groups. Each rat was weighed and labeled before treatment. A 7,12-Dimethylbenz[a]anthracene (DMBA) solution (in corn oil) was administered intraperitoneally (0.5 mL) every three days for four doses to induce tumors. Photodynamic therapy was applied using red light at 400 J/cm^2 for selected groups. All rats were monitored for behavior, health and tumor development. Post-treatment, animals were sacrificed for histopathological and biochemical analysis of tissues.

RESULTS AND DISCUSSION

Synthesis of gelatin nanoparticles: The synthesis of gelatin nanoparticles (GeNPs) was successfully achieved using the two-step desolvation method. The observed color change from pale yellow to dark brown during acetone addition indicated nanoparticle formation. This visual transformation confirms successful crosslinking and particle development, consistent with previous gelatin nanoparticle studies. The synthesized GeNPs were subjected to physicochemical and biological characterizations, including particle size, zeta potential, SEM, FTIR, XRD, DSC, TGA and biological evaluations to assess their anticancer potential.

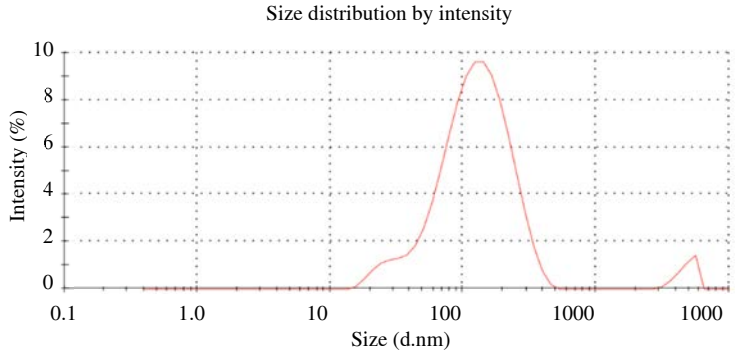

Fig. 1: Particle size distribution of formulation containing GeNP

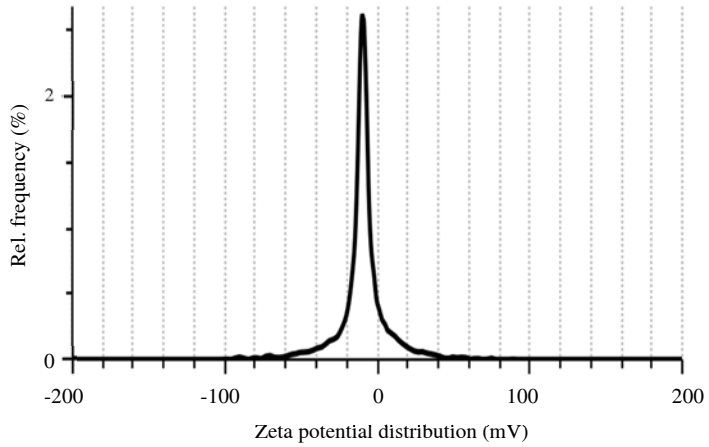

Fig. 2: Zeta Potential distribution of gelatin nanoparticle formulation

Particle size analysis: Dynamic Light Scattering (DLS) analysis revealed a Z-average particle size of 107.6 nm with an intercept value of 0.780, confirming a uniform size distribution. The particle size distribution analysis in Fig. 1 indicated three distinct peaks. Peak 1 at 137.5 nm (96.3% intensity), Peak 2 at 4808 nm (3.7% intensity) and Peak 3 at 0 nm (0% intensity). The predominant population of nanoparticles was within the nanoscale range, confirming successful synthesis. The presence of minor larger particles suggests minimal aggregation, which can occur during solvent evaporation or crosslinking.

Zeta potential analysis: The mean zeta potential of the synthesized GeNPs was recorded at -7.7 mV (SD±0.5), with the main distribution peak at -9.6 mV. This slightly negative surface charge indicates moderate colloidal stability, suggesting potential aggregation over time due to weak electrostatic repulsion. The electrophoretic mobility was -0.5100 µm·cm/Vs, confirming negatively charged surfaces. The optical density filter (3.1001) and conductivity (0.138 mS/cm) support accurate measurement conditions. Although moderately stable, further surface modification or addition of stabilizers could enhance long-term dispersion stability, especially for biomedical applications. Zeta Potential Distribution of Gelatin nanoparticle Formulation is shown in Fig. 2.

Scanning electron microscopy (SEM): SEM analysis of blank and drug-loaded formulations (SA24-3, Ce6, AS1411) revealed smooth, spherical particles within the nano range (<200 nm). Uniform particle morphology and absence of surface irregularities confirm controlled synthesis and appropriate crosslinking. These observations are consistent with DLS results, validating the successful fabrication of nano-sized, monodisperse gelatin nanoparticles suitable for drug delivery. Figure 3 shows the SEM image of blank nanoparticles, while the Fig. 4 shows the SEM image of SA24-3, Ce6 and AS1411 loaded nanoparticles. The SEM images prove that all the nanoparticles have a size of less than 200 nm.

Fourier transform infrared spectroscopy (FTIR): FTIR spectra of blank nanoparticles displayed characteristic peaks of gelatin: O-H stretching at 3350-3650 cm^{1} and C = O

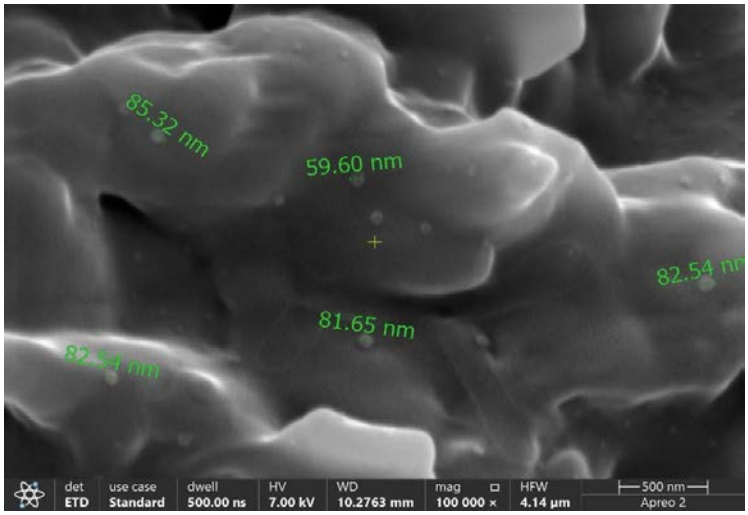

Fig. 3: SEM image of blank nanoparticles

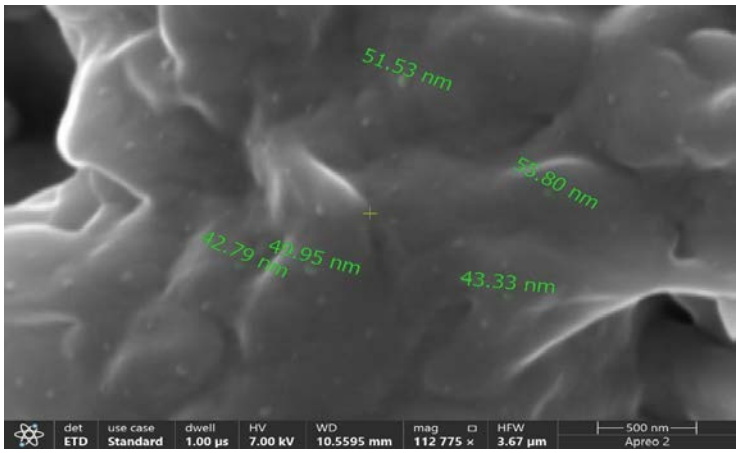

Fig. 4: SEM image of SA24-3, Ce6 and AS1411 loaded nanoparticles

stretching at 1210-1320 cm^{-1}, confirming polymer integrity. Ce6-loaded nanoparticles exhibited additional peaks between 3200-3500 cm^{-1} (O-H stretching) and at 1427 cm^{-1} (C-C stretching), along with a strong band at 1512 cm^{-1} attributed to mixed C = O and aromatic C-H vibrations. The AS1411 and SA24-3-loaded formulations showed distinctive C–N stretching at 1263 cm^{-1} and out-of-plane C-H bending between 690-900 cm^{-1}. Importantly, all formulations retained gelatin's characteristic peaks, verifying successful drug incorporation without polymer degradation. These spectral shifts indicate molecular interactions between the drugs and polymeric matrix. FTIR Spectrum of different Formulations are shown in Fig. 5.

X-ray diffraction (XRD): XRD analysis provided insights into the crystalline structure of the formulations[14]. The diffractograms of SA24-3, Ce6 and AS1411 displayed sharp peaks between 2θ = 5°-25° and 16°-26°, characteristic of their crystalline nature. In contrast, gelatin exhibited a broad halo, indicating an amorphous form. The XRD patterns of the nanoparticle formulations (F1-F5) showed the absence of sharp peaks, suggesting a transformation from crystalline to amorphous state upon encapsulation. This amorphous structure indicates successful drug entrapment within the gelatin matrix and improved solubility, as supported by Ramasamy *et al.*[15] with similar findings. X-ray diffractograms of formulations and their components are shown in Fig. 6.

Differential scanning calorimetry (DSC): The DSC thermogram of the blank formulation (F1) exhibited a sharp endothermic peak at 318.09°C, corresponding to gelatin melting. The drug-loaded formulation (F5) showed a peak at 299.71°C, indicating a shift due to molecular interactions between polymer and encapsulated components (Fig. 7). The reduction in melting point suggests physical entrapment and compatibility of the active compounds, which may enhance the thermal stability and homogeneity of the nanoparticles[16].

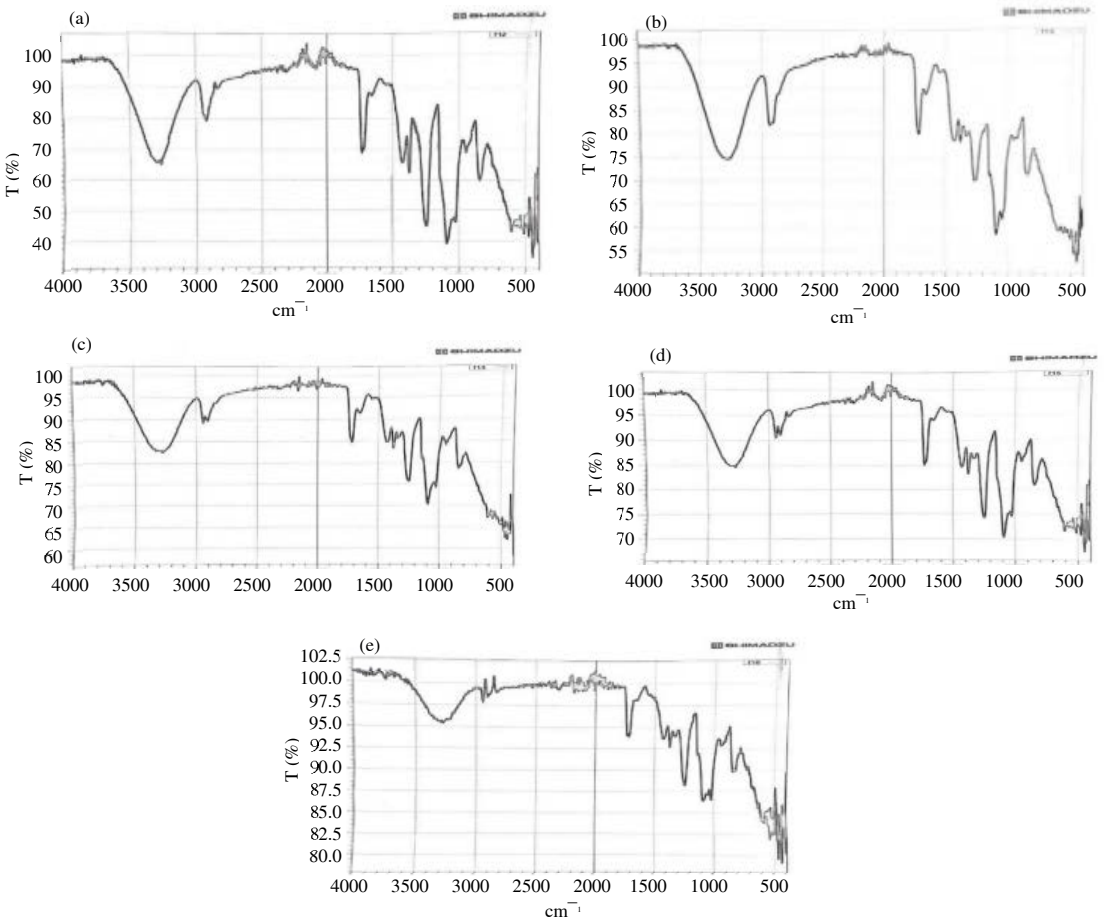

Fig. 5. FTIR Spectrum of different Formulations

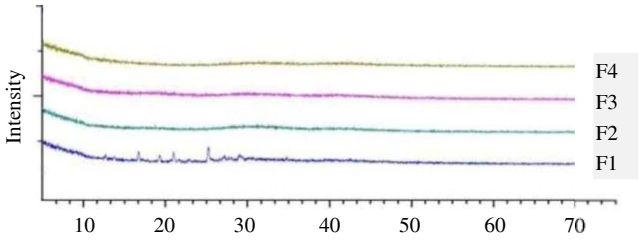

Fig. 6: X-ray diffractograms of formulations and their components

Thermogravimetric analysis (TGA): Figure 8 illustrates a weight loss of 15.619% at 283.96°C, followed by a significant mass reduction of 69.918% at 342.74°C. Similarly, the subsequent thermogravimetric curve demonstrates a weight loss of 15.706% at 267.13°C and a further loss of 60.632% at 332.55°C, indicating the thermal degradation behavior of the sample across these temperature ranges.

Erythrocyte aggregation test: The erythrocyte aggregation test demonstrated that blood samples treated with formulations F1-F5 under dark conditions exhibited no structural alterations or aggregation of red blood cells, indicating that the formulations remain inactive without photodynamic stimulation. However, upon exposure to red light for intervals ranging from one to five seconds, all formulations induced distinct RBC aggregation. This aggregation is considered advantageous, as it enhances oxygen delivery to the tumor microenvironment, which is essential for photodynamic therapy (PDT) to generate reactive oxygen species responsible for cancer cell destruction. The observed aggregation under light exposure

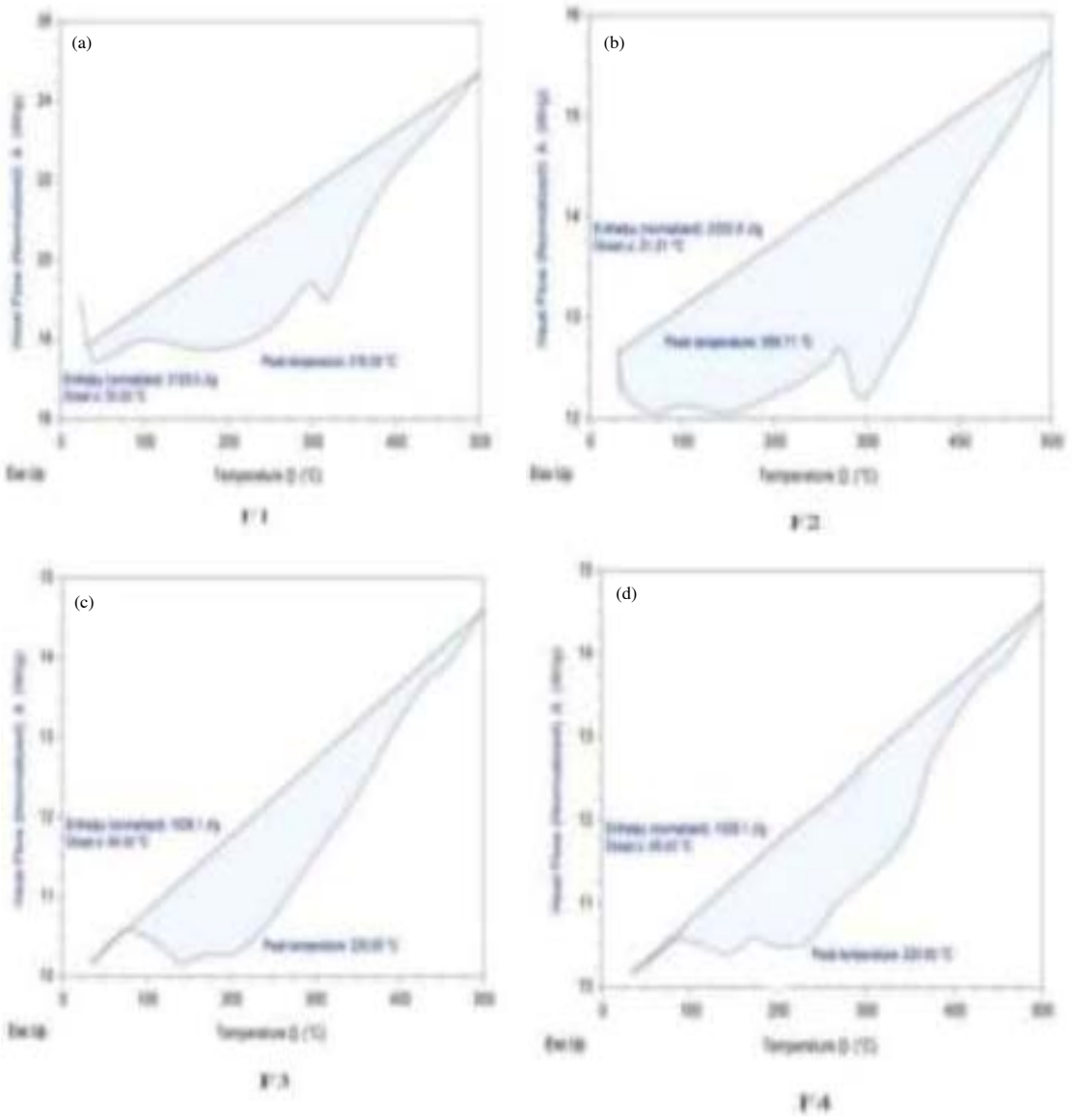

Fig. 7: DSC Analysis of reactant and formulations

suggests that controlled RBC aggregation may elevate local oxygen levels, thereby improving PDT efficacy[17]. The absence of aggregation in the dark and its occurrence only under light exposure confirm the photosensitive nature of the formulations, where therapeutic effects are activated exclusively by illumination at specific wavelengths (Fig. 9)[18].

***In vitro* cytotoxicity (MTT assay):** The cytotoxic potential of formulations F1–F5 was evaluated against MCF-7 breast cancer cells. Under dark conditions, F1 showed no significant cytotoxicity, indicating the non-toxic nature of blank nanoparticles. However, upon light exposure, all formulations exhibited significant cytotoxic effects compared to control. The cytotoxicity increased with light exposure duration, demonstrating the light-dependent therapeutic action of PDT. The combined action of Chlorin e6, which generates reactive oxygen species upon irradiation and SA24-3, an established anticancer compound, enhanced cell death. The aptamer AS1411 likely contributed to targeted delivery, increasing the overall efficacy.

CAM assay (anti-angiogenic activity): The CAM model was used to assess anti-angiogenic potential. The blank formulation (F1) produced no noticeable change in vascularization, confirming its inert nature. In contrast, formulation F5 (SA24-3+Ce6+AS1411) under light exposure significantly reduced blood vessel density and branching, indicating potent inhibition of angiogenesis. The suppression of vascular growth is attributed to the synergistic effects of PDT-induced oxidative stress and the anti-angiogenic activity of SA24-3, which inhibits VEGF expression[19]. These findings demonstrate the therapeutic potential of the combined formulation in reducing tumor vascularization and progression (Fig. 10).

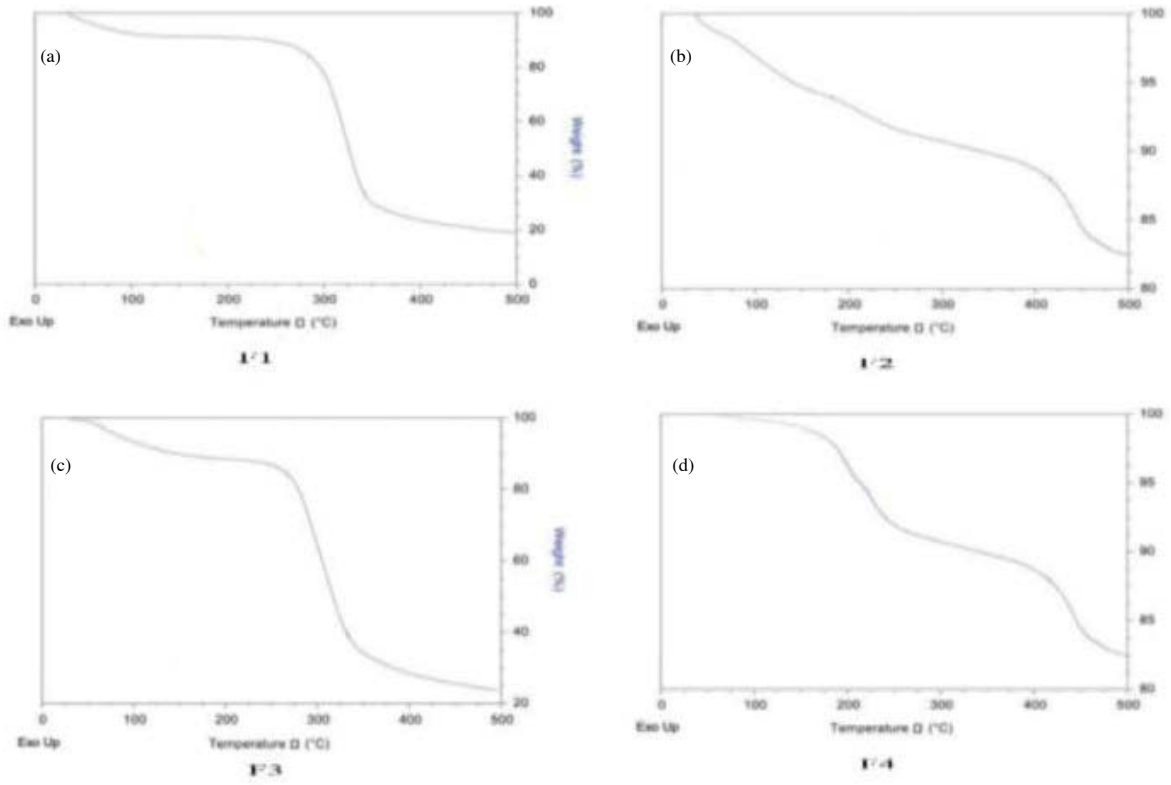

Fig. 8: TGA thermogram of Reactants and formulation

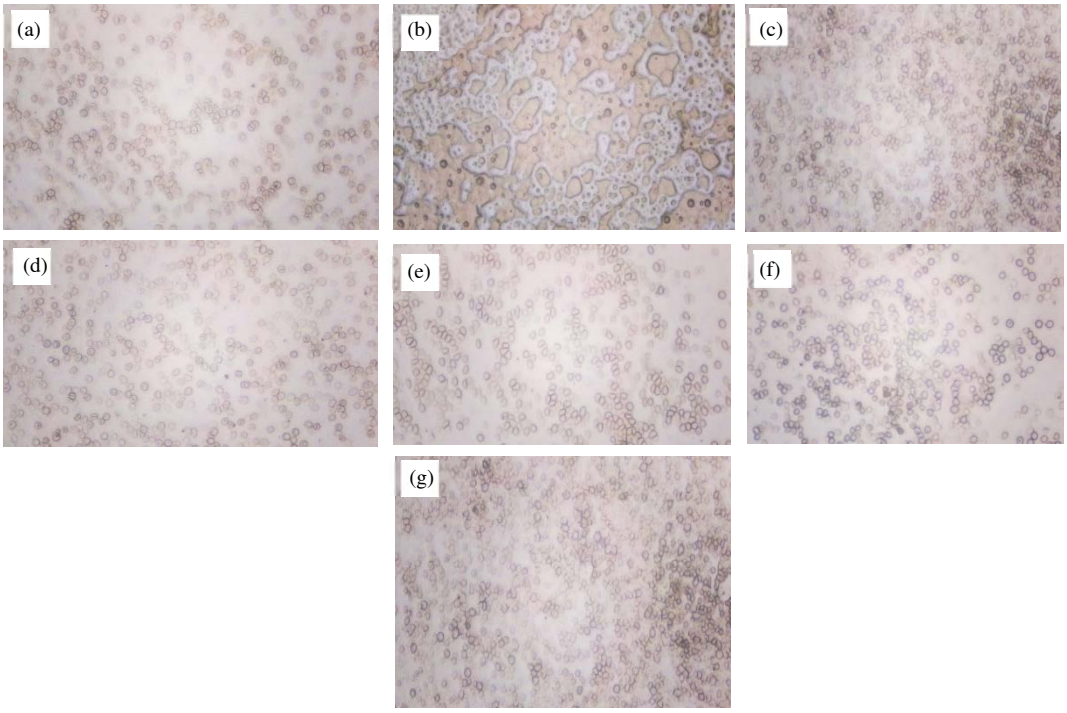

Fig. 9 (a-g): Erythrocyte aggregation test (a) RBCs slide images with normal saline, (b) RBCs slide images with triton x-100 (Positive Control), (c) RBCs slide images with F1, RBCs slide images with F2, RBCs slide images with F3, RBCs slide images with F4.

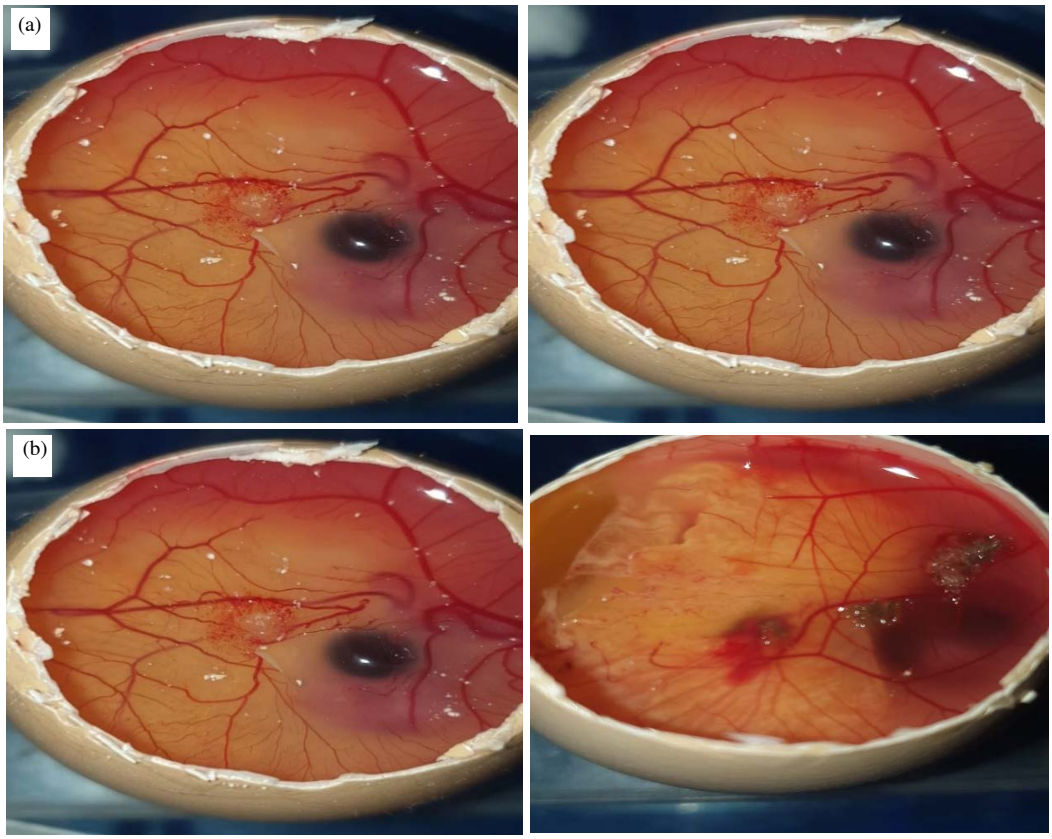

Fig 10 (a,b): Difference in vascularization of eggs before and after PDT (a) when treated with F1 formulation (b) when treated with F5 formulation

Table 1: Haematological analysis results of *in-vivo* study

Blood Tests	Control	F1	F2	F3	F4	F5	Units
Hemoglobin	13.8	12.9	12.4	14.2	11.4	12.6	g/dL
Platelets	787,000	883,000	866,000	920,000	966,000	986,000	million/cm
WBCs	8900	7100	6900	5400	6100	7400	/cmm
Neutrophils	34	32	38	30	18	35	%
Lymphocytes	64	66	60	69	80	79	%
Monocytes	01	01	01	00	01	01	%
Eosinophil	01	01	01	01	01	01	%

Hematological analysis: Hematological evaluation was performed to assess the effect of various formulations on blood cells under both dark and light (photodynamic) conditions. The results demonstrated that treatment induced hemolysis of Red Blood Cells (RBCs), as indicated by a reduction in hemoglobin (Hb) levels compared to the control. A decrease in Total Leukocyte Count (TLC) was also observed, suggesting a suppressed immune response, while an increase in platelet count indicated the onset of thrombocythemia. These findings collectively highlight the photodynamic influence and hematological alterations induced by the formulations (Table 1).

Serum biochemistry: As shown in Table 2, serum biochemical analysis indicated no significant differences in aspartate aminotransferase (AST), alanine aminotransferase (ALT), or alkaline phosphatase (ALP) levels between the treated and control groups, suggesting the absence of hepatocellular damage or necrosis[20]. Furthermore, total bilirubin, serum urea and creatinine levels did not show any notable increase, confirming that renal function remained unaffected by the treatment.

Histopathological examination: Histopathological evaluation was performed to examine the microscopic architecture of various organs. Histology, the study of cellular and tissue-level structures within organisms, provides critical insights into the relationship between biological organization and disease progression. It enables the identification of structural and functional alterations at subcellular, cellular, tissue and

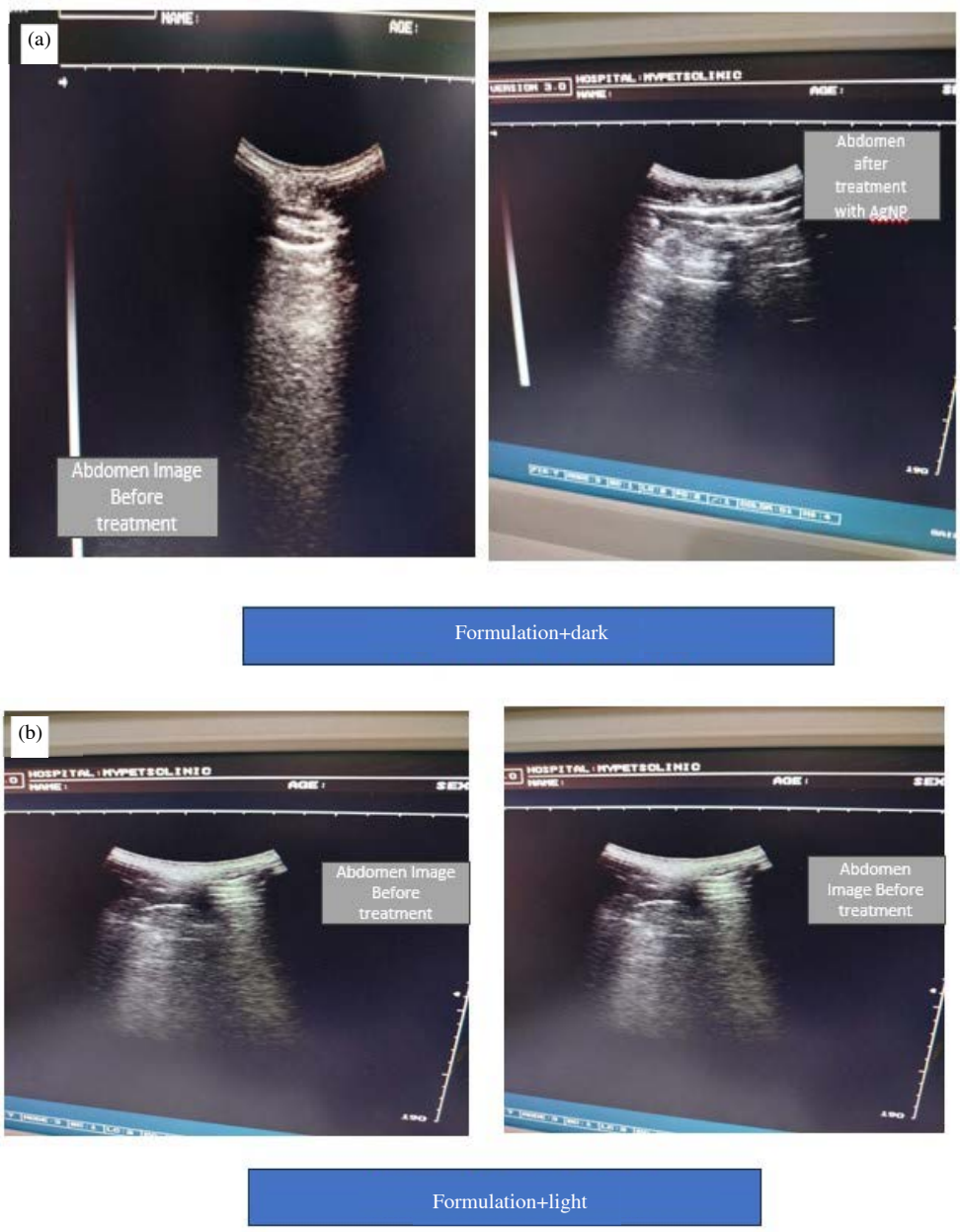

Fig. 11 (a,b): (a) Ultrasound analysis of tumors before and after treatment (b) Ultrasound analysis of tumors before and after treatment with F5 and red light

Table 2: Serum biochemistry results of *in-vivo* study

Blood tests	Control	F1	F2	F3	F4	F5	Units
Serum bilirubin-total	0.8	0.5	0.7	0.5	0.8	0.6	mg/dL
Serum ALT (SGPT)	39	17	36	21	31	27	µ/L
Serum alkaline phosphatase	221	141	189	137	199	156	µ/L
Serum urea	32	27	34	24	29	31	mg/dL
Serum creatinine	0.5	0.8	0.6	0.4	0.8	0.6	mg/dL

organ levels. Pathologists employ microscopic analysis to interpret histological images and recognize morphological features indicative of pathological conditions[13].

The renal tissues exhibited normal tubular brush borders, while the liver showed no evidence of parenchymal inflammation. Similarly, the cardiac and pulmonary tissues displayed no signs of deformity or necrosis. Overall, the histological analysis of major organs-including the lungs, liver, kidneys and heart-revealed normal anatomical features, with no significant pathological alterations observed in the control group.

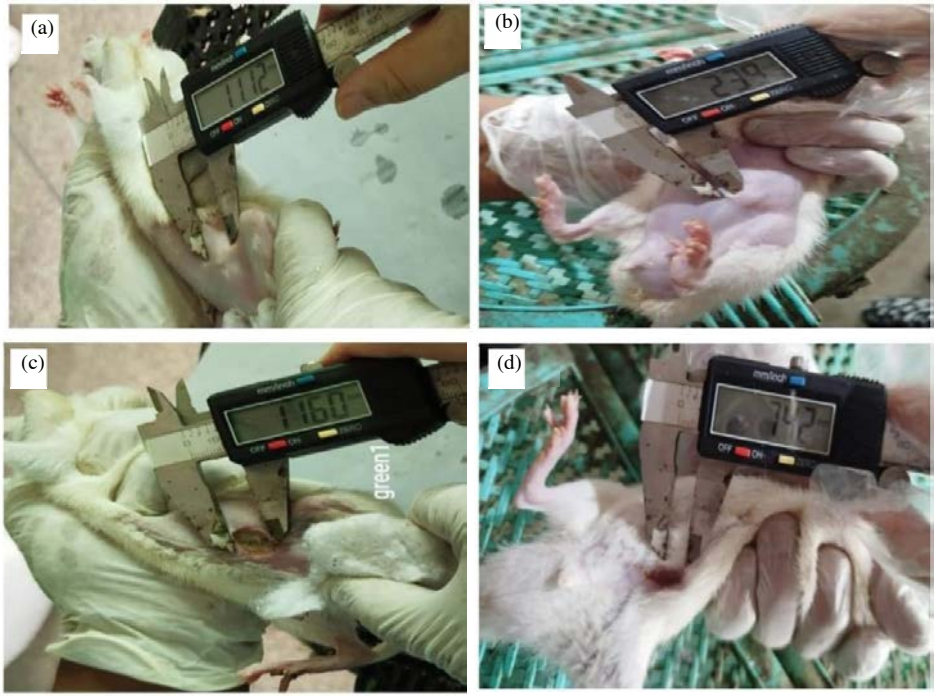

Fig. 12(a-d): Size of tumor in rats before and after treatment (a) Tumor size before treatment, (b) Tumor size after 4 weeks of treatment, (c) Tumor size before treatment+red light and (d) Tumor size after 4 weeks of treatment+red light

***In vivo* antitumor activity:** In Fig. 11a and b, ultrasound imaging was utilized to analyze tumor development in rats following DMBA induction. The analysis revealed the presence of fibrosis and cellular nuclei within the peritoneal region, confirming tumor formation prior to treatment with the formulated nanoparticles and light therapy.

Figure 11 illustrates the anti-tumor efficacy of formulation F5 under both dark and red light-assisted photodynamic treatment conditions. In rats treated with formulation F5 under dark conditions, the tumor size was significantly reduced from 11.12 mm to 2.79 mm within four weeks, demonstrating a pronounced anti-tumor response (Fig. 12). These findings indicate that formulation F5, incorporating SA24-3 and Ce6 and guided by the AS1411 aptamer, exhibits potent anti-tumor activity. However, further optimization is warranted to enhance its overall therapeutic performance.

CONCLUSION

This study successfully developed and optimized gelatin nanoparticles (GeNPs) loaded with SA24-3, Ce6 and AS1411 to enhance the anticancer efficacy of SA24-3 in breast cancer therapy using photodynamic therapy (PDT). Five formulations were prepared and evaluated for particle size and zeta potential, with Ce6 incorporated as a photosensitizer. The desolvation technique coupled with high-speed homogenization yielded nanoparticles with desirable therapeutic characteristics. The optimized formulation exhibited a particle size of 89.58 nm and a stable zeta potential of -20 mV. SEM analysis confirmed smooth, spherical morphology, while FTIR and XRD analyses indicated efficient drug loading with no crystalline peaks, confirming the amorphous nature of the nanoparticles.

The MTT assay revealed significant cytotoxicity against MCF-7 breast cancer cells, demonstrating strong anticancer potential. In the CAM model, the control formulation (F1) showed no effect on vascularization under PDT, while formulation F5 significantly reduced vascularization, confirming potent anti-angiogenic activity. RBC aggregation observed only under light exposure indicated enhanced oxygen delivery, a key factor in PDT efficiency.

In vivo results showed no significant alterations in blood parameters or tissue inflammation, indicating the formulation's safety. Overall, these findings highlight that AS1411-guided gelatin nanoparticles co-loaded with SA24-3 and Ce6 represent a promising, biocompatible and effective nanocarrier system for targeted breast cancer therapy, combining high therapeutic efficacy with excellent safety and warranting further clinical evaluation.

REFERENCES

1. Harbeck N, Penault-Llorca F, Cortes J, Gnant M, Houssami N, Poortmans P et al. Breast cancer. *Nat Revs Dis Primers*. [Internet]. 2019;5. Available from: https://doi.org/10.1038/s41572-019-0111-2

2. Rugo HS, Rumble RB, Macrae E, Barton DL, Connolly HK, Dickler MN et al. Endocrine therapy for hormone receptor–positive metastatic breast cancer: American society of clinical oncology guideline. *J Clin Oncol*. 2016;34:3069-3103.
3. Gadag S, Sinha S, Nayak Y, Garg S, Nayak UY. Combination therapy and nanoparticulate systems: Smart approaches for the effective treatment of breast cancer. *Pharmaceutics*. [Internet]. 2020;12(6). Available from: https://doi.org/10.3390/pharmaceutics12060524
4. Mansoori B, Mohammadi A, Doustvandi MA, Mohammadnejad F, Kamari F, Gjerstorff MF et al. Photodynamic therapy for cancer: Role of natural products. *Photodiagn Photodyn Ther*. 2019;26:395-404.
5. Hooshyar SP, Mehrabian RZ, Panahi HA, Jouybari MH, Jalilian H. Synthesis and characterization of pegylated dendrimers based on magnetic nanoparticles for letrozole extraction and determination in body fluids and pharmaceutical samples. *Microchem J*. 2018;143:190-197.
6. Yassemi A, Kashanian S, Zhaleh H. Folic acid receptor-targeted solid lipid nanoparticles to enhance cytotoxicity of letrozole through induction of caspase-3 dependent-apoptosis for breast cancer treatment. *Pharm Dev Technol*. 2020;25(4):397-407.
7. Sahrayi H, Hosseini E, Karimifard S, Khayam N, Meybodi SM, Amiri S et al. Co-delivery of letrozole and cyclophosphamide via folic acid-decorated nanoniosomes for breast cancer therapy: Synergic effect, augmentation of cytotoxicity and apoptosis gene expression. *Pharmaceuticals*. [Internet]. 2021;15(1). Available from: https://doi.org/10.3390/ph15010006
8. Khan MT, Uddin Z, Javed MA, Shah N, Bashir H, Shaikh AJ et al. PEGylated protamine letrozole nanoparticles: A promising strategy to combat human breast cancer via MCF-7 cell lines. *Biomed Res Int*. [Internet]. 2022;2022. Available from: https://doi.org/10.1155/2022/4438518
9. Priyadarsini S, Lahoti SR. RP-HPLC method development and validation for quantification of letrozole solid lipid nanoparticle. *J Res Pharm*. 2022;26(2):421-430.
10. Begines B, Ortiz T, Pérez-Aranda M, Martínez G, Merinero M, Argüelles-Arias F et al. Polymeric nanoparticles for drug delivery: Recent developments and future prospects. *NanoMater*. [Internet]. 2020;10(7). Available from: https://doi.org/10.3390/nano10071403
11. Gharieh A, Khoee S, Mahdavian AR. Emulsion and miniemulsion techniques in preparation of polymer nanoparticles with versatile characteristics. *Adv Colloid Interface Sci*. 2019;269:152-186.
12. Reddy NJ, Vali DN, Rani M, Rani SS. Evaluation of antioxidant, antibacterial and cytotoxic effects of green synthesized silver nanoparticles by Piper longum fruit. *Mater Sci Eng: C*. 2014;34:115-122.
13. Belsare AD, Mushrif MM. Histopathological image analysis using image processing techniques: An overview. *Signal Image Process : Int J*. 2012;3(4):23-36.
14. Shaban M, Ghaffary S, Hanaee J, Karbakhshzadeh A, Soltani S. Synthesis and characterization of new surface modified magnetic nanoparticles and application for the extraction of letrozole from human plasma and analysis with HPLC-fluorescence. *J Pharm Biomed Anal*. [Internet]. 2021;193. Available from: https://doi.org/10.1016/j.jpba.2020.113659
15. Ramasamy T, Tran TH, Choi JY, Cho HJ, Kim JH, Yong CS et al. Layer-by-layer coated lipid–polymer hybrid nanoparticles designed for use in anticancer drug delivery. *Carbohydr Polym*. 2014;102:653-661.
16. Amin J, Sharif M, Yasmin M, Fernandes SL. A distinctive approach in brain tumor detection and classification using MRI. *Pattern Recognit Lett*. 2020;139:118-127.
17. Meng Z, Xue H, Wang T, Chen B, Dong X, Yang L et al. Aggregation-induced emission photosensitizer-based photodynamic therapy in cancer: From chemical to clinical. *J Nanobiotechnol*. [Internet]. 2022;20. Available from: https://doi.org/10.1186/s12951-022-01553-z
18. Ding S, Wu W, Peng T, Pang W, Jiang P, Zhan Q et al. Near-infrared light excited photodynamic anticancer therapy based on UCNP@AIEgen nanocomposite. *Nanoscale Adv*. 2021;3(8):2325-2333.
19. Marinho MAG, Marques MDS, Cordeiro MF, Filgueira DDMVB, Horn AP. Combination of curcumin and photodynamic therapy based on the use of red light or near-infrared radiation in cancer: A systematic review. *Anti-cancer Agents Med Chem*. 2022;22(17):2985-2997.
20. Li J, Cai P, Shalviri A, Henderson JT, He C, Foltz WD et al. A multifunctional polymeric nanotheranostic system delivers doxorubicin and imaging agents across the blood–brain barrier targeting brain metastases of breast cancer. *ACS Nano*. 2014;8(10):9925-9940.